Title
Big insights from tiny peridotites: Evidence for persistence of Precambrian lithosphere beneath the eastern North China Craton

Authors
Liu, Jingao
Rudnick, Roberta L
Walker, Richard J
et al.

Publication Date
2015-05-01

DOI
10.1016/j.tecto.2014.05.009

Peer reviewed

Tectonophysics 650 (2015) 104–112

Contents lists available at ScienceDirect

Tectonophysics

journal homepage: www.elsevier.com/locate/tecto

Big insights from tiny peridotites: Evidence for persistence of Precambrian lithosphere beneath the eastern North China Craton

Jingao Liu [a,b,*], Roberta L. Rudnick [a], Richard J. Walker [a], Wen-liang Xu [c], Shan Gao [d], Fu-yuan Wu [e]

[a] Department of Geology, University of Maryland, College Park, MD 20742, USA
[b] Department of Earth and Atmospheric Sciences, University of Alberta, Edmonton, Alberta T6G 2E3, Canada
[c] College of Earth Sciences, Jilin University, Changchun 130061, China
[d] State Key Laboratory of Geological Processes and Mineral Resources, China University of Geosciences, Wuhan 430074, China
[e] State Key Laboratory of Lithospheric Evolution, Institute of Geology and Geophysics, Chinese Academy of Sciences, P.O. Box 9825, Beijing 100029, China

A R T I C L E I N F O

Article history:
Received 27 January 2014
Received in revised form 21 April 2014
Accepted 2 May 2014
Available online 10 May 2014

Keywords:
Osmium
Peridotites
Mantle xenoliths
Tan–Lu fault
Lithospheric thinning
North China Craton

A B S T R A C T

Previous studies have shown that the eastern North China Craton (NCC) lost its ancient lithospheric mantle root during the Phanerozoic. The temporal sequence, spatial extent, and cause of the lithospheric thinning, however, continue to be debated. Here we report olivine compositions, whole-rock Re–Os isotopic systematics, and platinum-group element abundances of small (<2 cm in maximum dimension) mantle peridotite xenoliths from two basalt localities from the eastern NCC, Wudi (Cenozoic) and Fuxin (Cretaceous). These locations lie far (~150–200 km) from the Tan–Lu fault, which has been linked to lithospheric replacement in the eastern NCC. Peridotites at both locations have fertile to moderately refractory compositions (Fo < 91.5), while highly refractory (Fo > 92) lithospheric mantle is largely absent. Osmium isotopic data suggest the Wudi peridotites experienced melt depletion primarily during the Paleoproterozoic (~1.8 Ga), although an Archean Os model age for one xenolith indicates incorporation of a minor component of Archean lithospheric mantle. These data suggest that a previously unrecognized Paleoproterozoic orogenic event removed and replaced the original Archean lithospheric mantle beneath the sedimentary basin at the southern edge of the Bohai Sea. By contrast, the Fuxin peridotites, entrained in Cretaceous basalts that crop out along the northern edge of the eastern NCC, document the coexistence of both ancient (≥2.3 Ga) and modern lithospheric mantle components. Here, the original Late Archean–Early Paleoproterozoic lithospheric mantle was, at least partially, removed and replaced prior to 100 Ma. Combined with literature data, our results show that removal of the original Archean lithosphere occurred within Proterozoic collisional orogens, and that replacement of Precambrian lithosphere during the Mesozoic may have been spatially associated with the collisional boundaries and the strike–slip Tan–Lu fault, as well as the onset of Paleo-Pacific plate subduction.

1. Introduction

The subcontinental lithospheric mantle forms the lower portion of continental plates and has been implicated in stabilizing continental crust, particularly within Archean cratons (Jordan, 1988). Studies of mantle xenoliths, carried to the surface in basalts and kimberlites, provide valuable insights into the composition and age of lithospheric mantle, and ultimately how and when it forms and how it has evolved (see Pearson et al., 2014, and references therein).

About two decades ago, it was recognized that the original Late Archean–Early Paleoproterozoic lithospheric mantle beneath the eastern portion of the North China Craton (referred to as eastern NCC) was removed and replaced by fertile, Phanerozoic lithospheric mantle sometime after the Ordovician (Griffin et al., 1998; Menzies et al., 1993). This is in contrast to the western NCC, which is characterized by rather thick lithosphere (>150 km; Chen, 2010; Tian et al., 2009) and, thus, is likely to still be dominantly underlain by original Archean–Paleoproterozoic lithospheric mantle. Since then, the eastern NCC has served as a natural laboratory for studying the loss of cratonic lithospheric mantle. Numerous geochemical and geophysical studies have sought to decipher the timing, extent and cause of lithospheric mantle removal and replacement (see reviews by Zhu et al., 2012a,b and references therein). Ancient lithospheric mantle that existed beneath the eastern NCC prior to thinning has been sampled in the form of mantle xenoliths from three diamondiferous, Ordovician kimberlites (Chu et al., 2009; Gao et al., 2002; Wu et al., 2006; Zhang et al., 2008a), which are located in the vicinity of the present-day Tan–Lu fault (Fig. 1). By contrast, peridotite xenoliths carried in spatially associated Cenozoic basalts have Re–Os systematics similar to modern convecting upper mantle (e.g., Chu et al., 2009; Gao et al., 2002; Wu

* Corresponding author at: Department of Earth and Atmospheric Sciences, University of Alberta, Edmonton, Alberta T6G 2E3, Canada. Tel.: +1 780 492 7725.
E-mail address: jingao@ualberta.ca (J. Liu).

http://dx.doi.org/10.1016/j.tecto.2014.05.009
0040-1951/

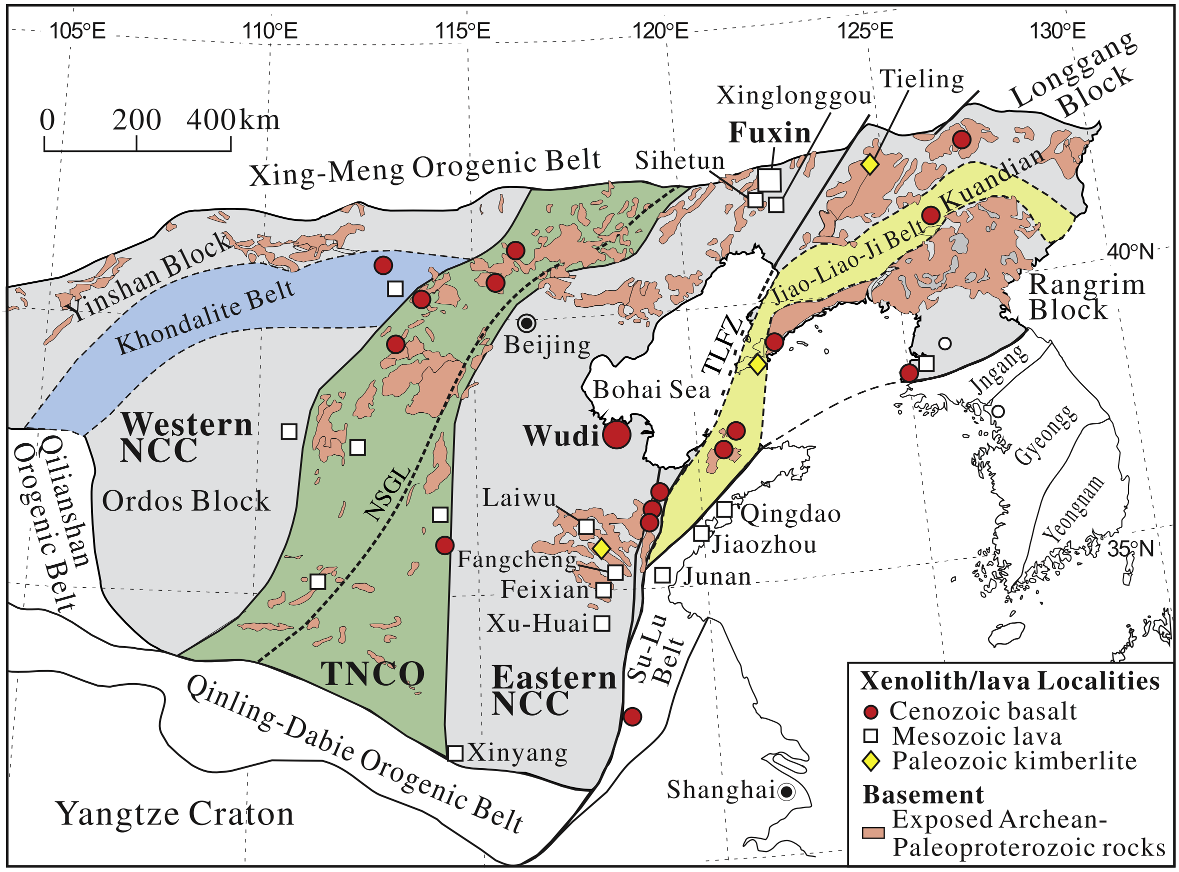

Fig. 1. Tectonic sketch map of the North China Craton (NCC), which is composed of the eastern NCC block, western NCC block, and the intervening Trans-North China Orogen (TNCO), with cross-cutting Paleoproterozoic fold belts: Khondalite Belt, western NCC, and Jiao-Liao-Ji Belt, eastern NCC (modified from Zhao et al., 2005). NSGL: North–South Gravity Lineament; TLFZ: Tan–Lu Fault Zone.

et al., 2003, 2006), implying removal and replacement of the original Late Archean–Early Paleoproterozoic lithospheric mantle following the Ordovician, most likely during the Mesozoic. However, studies of mantle xenoliths erupted in the Mesozoic (e.g., Gao et al., 2008), or spatially distant from the Tan–Lu fault (e.g., Wu et al., 2006) are few, largely due to the scarcity of samples, as well as the very small size of those that do occur. The study of additional Mesozoic-erupted mantle xenoliths may be useful in constraining the temporal sequence and extent of lithospheric thinning in the eastern NCC. More importantly, the Tan–Lu fault has been linked to lithospheric replacement in the eastern NCC (e.g., Xiao et al., 2010; Zhang et al., 2007), so it is critical to examine xenoliths that sample the mantle far removed from the fault in order to exclude possible effects imparted by it.

Here we report olivine compositions, whole-rock Re–Os isotopic systematics and platinum-group element (PGE) abundances of tiny xenolithic peridotites from two localities that lie ~150–200 km to the west of the Tan–Lu strike–slip fault in the eastern NCC. Combined with literature data, the results allow us to place new constraints on the spatial and temporal removal and replacement of the original Archean and Paleoproterozoic lithospheric mantle in the eastern NCC, with important implications for understanding the tectonic processes involved.

2. Geological settings and samples

The eastern NCC block formed through the collision of the northern Longgang and southern Rangrim blocks, forming the Paleoproterozoic (ca. 2.1–1.9 Ga) Jiao-Liao-Ji Belt (Fig. 1; e.g., Li et al., 2011). The composite eastern NCC block amalgamated with the western NCC block to form the NCC via a ~1.85 Ga continent–continent collision (Zhao et al., 2005). Long after stabilization, the NCC experienced massive circum-craton Phanerozoic subduction and collisional orogenies, manifested in several orogenic belts: the Early Paleozoic Qilianshan Orogen to the west, the Late Paleozoic Xing-Meng Orogenic Belt to the north, and the Late Permian to Triassic Qinling–Dabie–Sulu ultra-high pressure metamorphic orogenic belt to the south and east, as well as the Jurassic onset of the Paleo-Pacific Ocean plate subduction beneath eastern China (Xu et al., 2013a). The sinistral Tan–Lu strike–slip fault system likely formed following the collision of the Yangtze Craton and NCC during the Triassic, which led to the creation of the Qinling–Dabie–Sulu Belt (Yin and Nie, 1993). Since the Mesozoic, the eastern NCC has experienced extension and intraplate magmatism, the latter of which entrained the deep-seated mantle xenoliths examined in this study (Fig. 1).

The mantle xenoliths studied here are from Wudi (N38°0′36.3″ E117°40′51.8″) and Fuxin (N42°16′39.6″ E121°54′10.9″) (Fig. 1), and are all garnet-free spinel peridotites. Those from Wudi were entrained in Pleistocene (<1 Ma; Chen et al., 1985) alkali nephelinites from the interior of the eastern NCC. The elemental and isotopic characteristics of the Wudi host nephelinites indicate that these lavas were derived from low degrees of melting of the depleted asthenospheric mantle, hybridized with recycled crustal materials (Luo et al., 2009). The peridotites from Fuxin were entrained in the Cretaceous (~100 Ma; Zhang and Zheng, 2003) alkali basalts from the northern edge of the eastern NCC. The Fuxin host basalts have geochemical features similar to those of Cenozoic basalts that are interpreted to be derived from the depleted asthenosphere (Zhang and Zheng, 2003). Peridotites from both localities are dominantly spinel lherzolites with minor harzburgites, and are fresh, but small (<2 cm in maximum dimension), making interpretation of whole-rock Re–Os isotope and PGE abundance data challenging.

3. Analytical methods

3.1. Major element composition of olivines

Major element compositions of olivine grains separated from mantle xenoliths, including 82 peridotites from Wudi and 39 peridotites from Fuxin, were analyzed in order to assess the range of melt depletion exhibited by the peridotites. These analyses were carried out using wavelength dispersive spectroscopy with a 15 kV accelerating voltage, a 20 nA cup current, and a 10 μm diameter beam on a JEOL 8900 electron probe micro-analyzer (EPMA) at the University of Maryland (UMd). A variety of natural minerals were used as primary and secondary standards, and raw X-ray intensities were corrected using a ZAF algorithm. One to three spots per olivine grain, and one to four grains were analyzed per sample. Based on the forsterite contents (Fo $= 100 \times$ molar Mg/(Mg + Fe)) of olivine grains, a representative sub-suite of peridotites (11 of 82 Wudi peridotites and 16 of 39 Fuxin peridotites), spanning the range in Fo values, and also yielding sizable materials, were selected from each locality for whole-rock isotopic and elemental analyses.

3.2. Sample preparation

The lava enclosing each xenolith was initially removed using a diamond saw. The liberated xenolith was further purified by grinding, using a polisher with a coarse-grained, silicon carbide-coated paper. Each "lava-free" xenolith was rinsed with deionized Milli-Q water, dried at room temperature, then gently crushed to a coarse grain size, using an agate mortar and pestle. This material was inspected under a binocular microscope and any remaining visible pieces of lava were removed. The virtually lava-free, coarse peridotite fragments were then pulverized to fine powders using an agate mortar and pestle. The selected Wudi and Fuxin peridotites yielded 0.10 to 0.36 and 0.08 to 1.4 g of powders, respectively, for bulk analyses.

3.3. Whole-rock Re–Os isotope and PGE abundance analyses

Appropriate amounts of mixed ^{185}Re–^{190}Os and ^{191}Ir–^{99}Ru–^{194}Pt–^{105}Pd spikes and sample powders (0.09 to 0.26 g for Wudi peridotites and 0.08 to 0.51 g for Fuxin peridotites) were sealed, along with 2 ml of concentrated Teflon-distilled HCl and 3.5 ml of concentrated Teflon-distilled HNO_3 into a pre-cleaned, chilled, thick-walled borosilicate Carius tube, and heated to 270 °C for >72 h. Osmium was extracted immediately from the acid solution after digestion by solvent extraction into CCl_4, then back extracted into HBr (Cohen and Waters, 1996), and finally purified via microdistillation using a H_2SO_4–dichromate solution into 15 μl of concentrated HBr (Birck et al., 1997). Iridium, Ru, Pt, Pd and Re were separated and purified from the remaining acid solution using anion exchange column chromatography (Rehkämper and Halliday, 1997).

Osmium isotopic compositions were determined as OsO_3^- by peak jumping, using a single electron multiplier on the UMd Thermo Triton thermal ionization mass spectrometer in negative ionization mode. Raw ratios were first reduced by oxygen correction using $^{17}O/^{16}O = 0.0003749$ and $^{18}O/^{16}O = 0.0020439$ (Nier, 1950), followed by spike correction using a mass balance equation and the spike isotope composition, and finally by instrumental mass fractionation correction using $^{192}Os/^{188}Os = 3.083$ (Walker et al., 2005) via the exponential law. The Os concentration of each sample was determined by isotope dilution. The internal precision on $^{187}Os/^{188}Os$ ratios was typically better than 0.2% (2σ). The reported $^{187}Os/^{188}Os$ ratios of samples were corrected for instrumental bias, typically less than 0.1%, using the correction factor that was calculated by dividing the recommended ratio of 0.11379 by the average measured $^{187}Os/^{188}Os$ of the UMd Johnson Matthey Os reference material for each analytical session.

All Re and PGE column cuts were dissolved in 5% HNO_3 and measured using a single electron multiplier on an Element 2 ICP–MS at UMd. For the Ir and Pt analyses, a hafnium (^{178}Hf) standard solution was measured to determine the oxide production rate (HfO/Hf, which was less than 0.2%) in order to correct for possible Hf oxide isobaric interferences. Given that the $^{178}Hf^+$ signals were less than a few thousand counts per second in the sample solutions, the Hf oxide isobaric interference correction was negligible for Ir and Pt. For the Pd analysis, yttrium (^{89}Y) and zirconium (^{90}Zr) standard solutions were measured to determine the oxide production rate (MO^+/M^+), which was generally less than 0.5%. Given very low signals (less than 2000 cps) of $^{89}Y^+$ in the sample solutions, the calculated signals of $^{89}YO^+$ were negligible for isobaric interference on mass 105; by contrast, the isobaric interference correction of $^{90}ZrO^+$ on mass 106 was as high as 5%, depending upon Zr/Pd ratios in the sample solutions. Instrumental mass fractionation was corrected for by periodic measurements of in-house standards (usually one per three sample analyses) using the standard bracketing method, resulting in normally less than 3% correction. Diluted, spiked solutions of the iron meteorites South Byron (for Ir and Pt), Dronino (for Re), and Sikhote-Alin (for Ru) were run during each analytical session as secondary standards. No Pd meteorite aliquots were run. The isotopic ratio results of these runs are within 2% with accredited values obtained from precise measurements of undiluted sample solutions using Faraday cups of a Nu Plasma ICP–MS (see Table S1 in the Electronic Supplement).

During the analytical campaign, two blanks were processed and yielded the following average quantities: Os 0.29 pg, Ir 0.77 pg, Ru 2.9 pg, Pt 5.0 pg, Pd 4.1 pg, and Re 0.76 pg. Due to small sample size, blank corrections for samples vary from insignificant to a few percent for Os (0.04–1.0%), Ir (0.03–2.7%, except for 11.9% for sample FW1-22), Ru (0.1–4.0%), Pt (0.04–7.9%, except for 65% for sample FW1-22), and Pd (0.1–5.5%, except for 10.0% for sample FW1-22), while the blank constitutes between 0.3 and 40% of the total Re in the samples.

4. Chemical and isotopic compositions and the age of the lithospheric mantle

Full major element data for olivines are provided in the Electronic Supplement (Table S2). Olivines from Wudi peridotites have forsterite contents (Fo) ranging from 89.1 to 92.3, with an average of 90.5 ± 0.7 (1σ; n = 82; Fig. 2). Olivines from Fuxin peridotites are characterized by a significantly larger range of Fo, from 82.6 to 92.2 (n = 54; Zheng et al., 2007; this study), with two harzburgite samples having Fo > 92, and 12 lherzolites having Fo < 88. Most of the peridotites from both Wudi and Fuxin have olivines with lower Fo compared to typical Archean cratonic peridotites (Fig. 2). Given that typical mantle peridotites have Fo ≥ 88 (Pearson et al., 2014, and references therein), the Fuxin lherzolites with Fo < 88 must have resulted from melt–peridotite interaction that led to Fe enrichment, greatly lowering Fo values.

The Re–Os isotope and PGE abundance data of the eleven Wudi and sixteen Fuxin peridotites are provided in Table 1. Both Wudi and Fuxin peridotite suites are characterized by large variations in PGE and Re concentrations. For example, Ir concentrations range from 0.17 to 2.25 and 0.09 to 7.24 ppb, respectively. The primitive upper mantle (PUM)-normalized patterns of the Wudi peridotites are characterized by PUM-like relative abundances to significant depletions in the platinum-group PGE (PPGE: Pt and Pd), relative to the iridium-group PGE (IPGE: Os, Ir and Ru) (Fig. 3a). Such patterns are consistent with variable degrees of melt extraction from residues, as shown by correlations between, for example, Pd/Ir and Fo values (Fig. 4). It is noted that the sample W50 shows prominent Re enrichment relative to IPGE, as reflected by a high $^{187}Re/^{188}Os$ of 3.67 (Table 1). Because the high Re/Os of the sample is inconsistent with its relatively low $^{187}Os/^{188}Os$ ratio of 0.1207, the Re enrichment must have occurred recently, most likely just before or during the eruption event. Despite having $^{187}Os/^{188}Os$ (0.1176 to 0.1304)

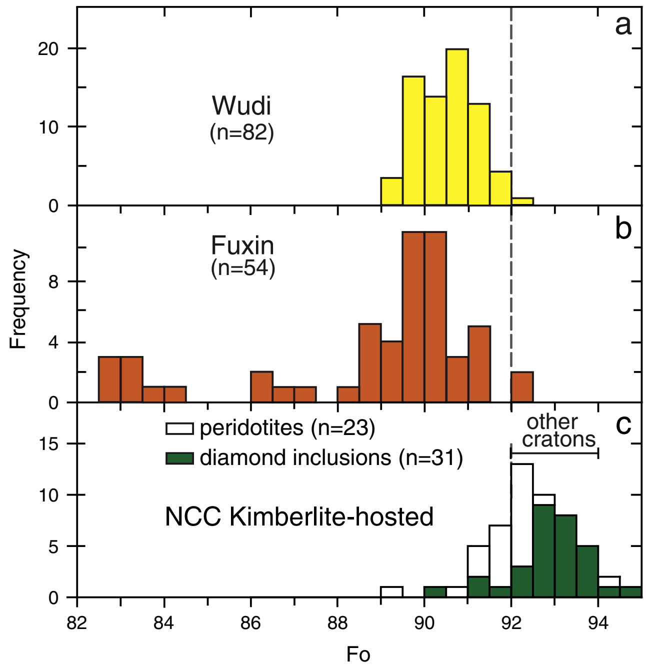

Fig. 2. Histograms of average forsterite contents (Fo = 100 × mol Mg/(Mg + Fe)) of olivines from individual xenolithic peridotites and diamond inclusions. Each datum represents the value for a single sample, which represents between 1 and 12 spot analyses. a) Wudi; b) Fuxin (16 samples from Zheng et al., 2007, and 38 from this study); and c) olivines from xenolithic peridotites and diamonds in Ordovician kimberlites from the eastern NCC (data from Zheng, 1999) and from other cratons (bar) (Pearson et al., 2014, and references therein).

within the range of modern samples from the convecting upper mantle, the Wudi peridotites show strong correlations between $^{187}Os/^{188}Os$ and melt depletion indicators, such as Pd/Ir ratio (Fig. 5a) and Fo content (Fig. 5b). Such correlations suggest that these rocks formed by an ancient melt depletion event, assuming that the mantle source was homogeneous in terms of Os isotopic composition and Re–PGE relative abundances. Assuming that no Re remains in residual peridotites at Fo = 92.5 ± 0.5 (such high forsterite contents suggest that the peridotites are residues after high degrees (>25%) of mantle partial melting (Bernstein et al., 2007) where nearly all Re is extracted into the melts (Handler et al., 1997)), the $^{187}Os/^{188}Os$ vs. Fo correlation yields an initial $^{187}Os/^{188}Os$ of 0.1146 ± 0.0020 for the suite, which gives an Os model age of 1.8 ± 0.3 Ga using the method of Shirey and Walker (1998). The harzburgite sample W66, which has the highest Fo of 92.3 and lowest $^{187}Os/^{188}Os$ of 0.1099, yields an older T_{RD} Os model age of 2.5 Ga. In summary, the Wudi peridotites are consistent with a Paleoproterozoic formation age of 1.8 ± 0.3 Ga, but also with additional evidence for minor relicts of Archean lithospheric mantle.

In contrast to the Wudi peridotites discussed above, peridotites from Fuxin display diverse PUM-normalized PGE patterns (Fig. 3b–c), indicating that they experienced a more complicated history. Using these patterns, combined with their Os isotopic compositions, the Fuxin peridotites can be divided into four groups: Group 1, Re–PPGE depletion relative to IPGE with low $^{187}Os/^{188}Os$ of 0.1117 to 0.1174; Group 2, Re–PPGE depletion relative to IPGE with high $^{187}Os/^{188}Os$ greater than 0.1214; Group 3, relatively flat PGE patterns also with high $^{187}Os/^{188}Os$; and Group 4, Re–PPGE enrichment relative to IPGE with high $^{187}Os/^{188}Os$. Such diverse patterns are consistent with their large range of Fo values mentioned above. The Group 1 low-$^{187}Os/^{188}Os$ samples are all characterized by high Fo > 91, and prominent depletions of Re–PPGE relative to IPGE (Fig. 3b; Fig. 4), reflecting the antiquity of their mantle partial melting and minimal secondary overprinting. Despite having Re–PPGE depletion characteristics similar to the Group 1 samples, the Group 2 samples have much lower Fo, ranging from 88.1 to 90.4. The degrees of mantle partial melting inferred from such low Fo are unlikely to be responsible for the observed Re–PGE patterns (Fig. 3b; Fig. 4). This implies that the low Fo values of the Group 2 samples were likely caused by melt–peridotite reaction that caused Fe enrichment, which, however, little changed the Re–PGE system. Of note within this group, sample 11FW1-1, which has a Fo of 90.4, also has the highest $^{187}Os/^{188}Os$ of 0.2043 in the suite. This xenolith is likely to have experienced significant enrichment in radiogenic Os as a consequence of melt–peridotite reaction. This sample has a low Os concentration (0.86 ppb, Table 1) relative to the rest of the suite, making it particularly susceptible to isotopic modification.

The Group 3 samples are characterized by relatively flat PUM-normalized PGE patterns, which seem to be in accordance with limited degrees of partial melting based on their low Fo (87.4 to 90.3). However, three of the five samples in this group have remarkable depletions of Re relative to PGE (Fig. 3c). For instance, sample JG-33, with a Fo of 87.4, has a low $^{187}Re/^{188}Os$ of 0.066 that is inconsistent with its PUM-like Pd/Ir of 2.14 (Table 1). Such inconsistency implies that secondary overprinting (i.e., Fe enrichment, melt–peridotite reaction) generated the low Fo values; such melt–peridotite reaction in these rocks might have also caused the observed enrichment of PPGE but not Re, or depletion of Re but not PPGE. Group 4 samples display prominent PPGE enrichment relative to IPGE, as well as lesser degrees of Re enrichment (Fig. 3c), again suggesting melt–peridotite reaction. Combining the data from both Groups 3 and 4 samples, we conclude that melt–peridotite reaction caused the enrichment of PPGE and more limited Re enrichment relative to IPGE. Collectively, for all the high-$^{187}Os/^{188}Os$ samples (Groups 2, 3 and 4), the melt–peridotite reaction is manifested as Fe-enrichment and variable disturbance of Re–Os isotopic and PGE systematics of these rocks. The effects range from insignificant to strong enrichments of PPGE and Re relative to IPGE, as well as the modification of Os isotope ratios in low-Os samples. Similar or greater degrees of disturbance are expected to have occurred in samples with very low Fo (<88 indicative of more Fe enrichment), many of which were not analyzed for Re–Os isotopes and PGE abundances due to size limitations. Given that the high-$^{187}Os/^{188}Os$ samples have $^{187}Os/^{188}Os$ ratios mostly within the range of convecting upper mantle (0.1214 to 0.1357, with one having a ratio of 0.2043; Fig. 5; Table 1), the melt–peridotite reactions are presumed to have occurred recently, probably shortly before or during the eruption event, consistent with the juvenile nature of these rocks, as discussed below.

The initial $^{187}Os/^{188}Os$ (i.e., $^{187}Os/^{188}Os_{i,100\ Ma}$) for the Fuxin peridotites (calculated using measured Re/Os at 100 Ma) fall into two classes: low $^{187}Os/^{188}Os$ of 0.1117 to 0.1173 (Group 1), and high $^{187}Os/^{188}Os$ of 0.1212 to 0.1335 (Groups 2, 3 and 4), with one additional sample (Fo = 90.4) having an initial $^{187}Os/^{188}Os$ of 0.2041. The low-$^{187}Os/^{188}Os$ samples have Re-depletion (T_{RD}) Os model ages ranging from 1.5 to 2.3 Ga (Table 1, Fig. 5), similar to those of the Tieling xenoliths carried in a proximal Paleozoic kimberlite (1.7 to 2.3 Ga; Wu et al., 2006; Fig. 1). The model ages document the antiquity of the partial melting event(s) that generated these rocks. Considering that T_{RD} model ages mark the minimum age of peridotite partial melting, these mantle peridotites, as a whole, must be at least 2.3 Ga old. By contrast, the high-$^{187}Os/^{188}Os$ samples have low Fo values (<90.4), and their $^{187}Os/^{188}Os$ ratios generally plot within the range of modern convecting upper mantle (Fig. 5; Table 1). These rocks show no obvious correlation between Os isotopic composition and indicators of melt depletion (Fig. 5). Although most of them experienced recent Fe-enrichment from melt–peridotite reaction, this process might not have significantly modified the Os isotope ratios of most samples, which have relatively high Os concentrations (e.g., >1 ppb; Table 1). These lines of evidence suggest that the high-$^{187}Os/^{188}Os$ peridotites most likely represent recent additions to the lithospheric mantle. Consequently, at Fuxin, the new Os data indicate that both ancient (≥2.3 Ga) and young lithospheric mantle components coexisted at 100 Ma, and significant melt–

Table 1
Rhenium–Os isotopic compositions and platinum-group element (PGE) abundances of the Wudi and Fuxin peridotites from the eastern North China Craton.

Sample	Wt.	Os	Ir	Ru	Pt	Pd	Re	$^{187}Re/^{188}Os$	$^{187}Os/^{188}Os$	$(^{187}Os/^{188}Os)_i$	Pd/Ir	T_{RD}	T_{MA}	Fo
	g	ppb	ppb	ppb	ppb	ppb	ppb					Ga	Ga	
Wudi peridotites with an eruption age of <1 Ma														
W2	0.141	2.20	1.88	2.33	6.26	1.00	0.107	0.233	0.11966	0.11966	0.53	1.09	2.56	91.1
W8	0.153	2.36	2.25	2.65	2.70	1.19	0.028	0.065	0.12134	0.12134	0.53	0.84	1.00	91.3
W14A	0.093	0.36	0.41	0.62	0.81	0.52	0.036	0.61	0.12918	0.12918	1.26	−0.33	0.61	90.4
W27B	0.231	0.81	0.74	1.30	1.80	1.08	0.054	0.45	0.12587	0.12587	1.46	0.17	−1.46	89.5
W34	0.126	1.38	0.92	1.34	1.14	0.78	0.027	0.14	0.12261	0.12261	0.84	0.65	1.00	90.5
W37C	0.194	0.65	0.45	0.84	0.44	0.22	0.023	0.28	0.12241	0.12241	0.48	0.68	2.26	90.4
W50	0.260	0.81	0.70	1.22	1.57	0.59	0.616	3.67	0.12068	0.12068	0.84	0.94	−0.12	91.0
W54	0.172	1.18	1.15	1.67	1.51	0.41	0.052	0.21	0.11764	0.11764	0.36	1.38	2.87	91.5
W62	0.136	0.15	0.17	0.49	0.35	0.09	0.029	0.91	0.13042	0.13042	0.52	−0.51	0.40	91.1
W71	0.087	0.99	0.96	1.75	1.92	1.96	0.079	0.43	0.12814	0.12814	2.04	−0.17	2.19	89.3
W66	0.202	1.38	0.77	1.15	0.21	0.021	0.025	0.087	0.10994	0.10994	0.027	2.50	3.16	92.3
Fuxin peridotites with an eruption age of ~100 Ma														
Low $^{187}Os/^{188}Os$ group														
JG-15	0.193	1.54	2.31	3.12	2.66	1.01	0.059	0.18	0.11277	0.11246	0.44	2.13	3.80	91.0
FW1-29	0.172	2.40	2.46	3.88	2.43	1.20	0.034	0.069	0.11738	0.11726	0.49	1.44	1.71	91.1
FW1-30	0.237	4.47	4.96	6.85	6.26	2.57	0.058	0.062	0.11717	0.11706	0.52	1.47	1.71	91.2
FW1-46	0.229	6.61	7.24	16.9	6.36	2.49	0.015	0.011	0.11170	0.11168	0.34	2.25	2.31	91.2
11FW1-12	0.077	1.63	2.40	1.42	1.53	0.53	0.028	0.082	0.11402	0.11388	0.22	1.93	2.39	91.4
High $^{187}Os/^{188}Os$ group														
JG-14	0.513	3.52	3.10	6.23	6.36	5.04	0.232	0.318	0.12493	0.12440	1.63	0.39	1.46	90.3
JG-25	0.319	3.14	2.81	5.87	2.94	1.47	0.070	0.11	0.12826	0.12808	0.52	−0.16	−0.26	88.1
JG-33	0.213	2.32	1.83	3.76	4.02	3.92	0.032	0.066	0.12759	0.12748	2.14	−0.07	−0.11	87.4
JG-52	0.155	0.131	0.104	0.80	6.66	1.77	0.044	1.6	0.12849	0.12580	17.1	0.18	0.07	88.6
JG-55	0.386	1.81	2.64	2.01	22.9	21.9	0.431	1.30	0.13570	0.13354	8.30	−0.98	0.58	89.4
FW1-15	0.173	1.83	2.35	5.8	7.06	1.99	0.051	0.14	0.12394	0.12371	0.85	0.49	0.69	89.6
FW1-22	0.102	0.13	0.09	0.78	0.03	0.21	0.032	1.15	0.13067	0.12876	2.45	−0.26	0.29	89.9
FW1-27	0.141	3.02	2.31	4.00	1.25	0.65	0.024	0.038	0.12456	0.12449	0.28	0.37	0.40	89.5
11FW1-1	0.268	0.86	0.46	1.02	0.29	0.29	0.019	0.11	0.20431	0.20413	0.62	−12.79	−18.34	90.4
11FW1-26	0.360	1.87	2.66	3.59	6.17	5.20	0.023	0.060	0.12769	0.12758	1.95	−0.09	−0.12	89.1
11FW1-29	0.197	2.59	2.69	4.11	8.59	5.39	0.066	0.12	0.12138	0.12117	2.00	0.86	1.20	89.7

Note: Wt: weight, the amount of powder processed. The parameters used in model age calculations are: $\lambda_{Re} = 1.666 \times 10^{-11}$/year, $(^{187}Re/^{188}Os)_{CI} = 0.402$, and $(^{187}Os/^{188}Os)_{CI,0} = 0.1270$ (Shirey and Walker, 1998). $(^{187}Os/^{188}Os)_i$ is calculated at the time of host basalt eruption using the measured $^{187}Re/^{188}Os$. Fo: forsterite content (molar Mg/(Mg + Fe^{2+}) × 100) of olivines.

peridotite reaction occurred prior to eruption (100 Ma). Considering that no clear correlation is observed between calculated equilibrium temperatures and Fo values in the Fuxin peridotites (Zheng et al., 1999), we infer that the two generations of lithospheric mantle may, therefore, be interleaved at depth.

5. Tectonic implications

Mantle peridotites from Paleozoic through to Cenozoic lavas in the eastern NCC show considerable variation in chemical composition and age (e.g., Gao et al., 2002; Wu et al., 2006). Combining our new data with data from the literature, we discuss the tectonic processes operating within the eastern NCC during the Proterozoic and Phanerozoic eons (see summary in Table 2).

5.1. Proterozoic lithospheric replacement

The spatial juxtaposition of Archean crust (Wu et al., 2005) and underlying Archean lithospheric mantle, sampled by Ordovician kimberlitic xenoliths in the eastern NCC (Chu et al., 2009; Gao et al., 2002; Wu et al., 2006; Zhang et al., 2008a), provides strong evidence that the lithospheric mantle underlying these locations initially formed during the Archean, most likely related to the generation of the overlying continental crust. Yet such ancient lithospheric mantle is not observed in the mantle xenolith suites carried in Cenozoic basalts that erupted in the vicinity of the Ordovician kimberlites (Chu et al., 2009; Gao et al., 2002; Wu et al., 2003, 2006). By contrast, the Os isotopic data for the Wudi peridotites suggest that the lithospheric mantle underlying the central Bohai Sea, ~150 km to the west of the Tan–Lu fault was primarily formed during the Paleoproterozoic (~1.8 Ga), with minor Archean remnants. The basement geology of this region, however, is buried beneath Cretaceous and younger sedimentary rocks that accumulated within the Bohai Sea basin so it is unknown whether Paleoproterozoic or Archean crust currently underlies this region. Assuming that this portion of the eastern NCC originally formed during the Archean, our data suggest that a major portion of the original Archean lithospheric mantle was removed and replaced during the Paleoproterozoic. Elsewhere in the NCC, Paleoproterozoic lithospheric mantle is found below Archean crust that experienced collisional orogeny during the Paleoproterozoic (e.g., northern Trans-North China Orogen, Liu et al., 2010, 2011, 2012; Khondalite Belt, Liu et al., 2011; Jiao-Liao-Ji Belt, Wu et al., 2006; Fig. 1). By inference, we postulate that a similar Paleoproterozoic belt underlies the Wudi locality. Furthermore, the Paleoproterozoic lithospheric mantle in this region was evidently not entirely removed by subsequent Mesozoic processes.

5.2. Phanerozoic lithospheric replacement

In the eastern NCC, mantle xenoliths carried to the surface during the Cenozoic have distinct chemical compositions and ages compared to those carried by Ordovician kimberlites. This observation has been interpreted to suggest significant thinning and replacement of the lithospheric mantle during the Mesozoic (Chu et al., 2009; Gao et al., 2002; Griffin et al., 1998; Menzies et al., 1993; Wu et al., 2003). On the northern edge of the eastern NCC, the Fuxin peridotites sample fragments of both ancient (≥2.3 Ga) and modern lithospheric mantle present at 100 Ma.

On the northern margin of the NCC, Late Paleozoic collision between the Siberian Craton and the NCC formed the Xing-Meng Orogenic Belt through shortening and thickening of the lithosphere. This was followed by extension, as seen by the emplacement of metamorphic core complexes in the Early Cretaceous (120–107 Ma; Yang et al., 2007).

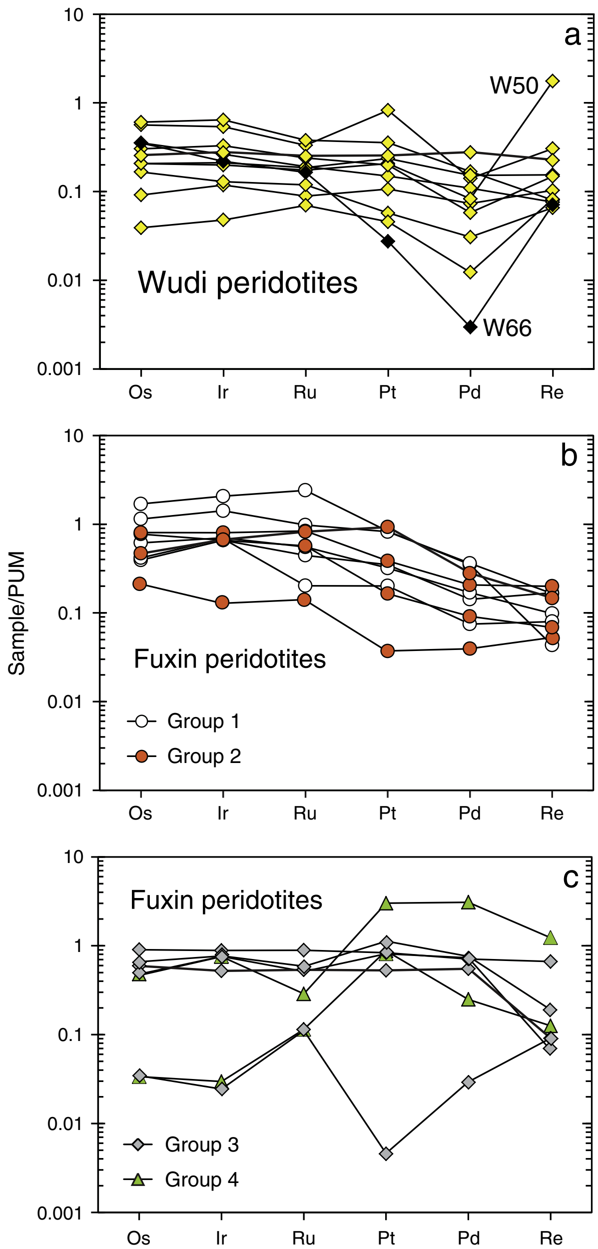

Fig. 3. Primitive-upper-mantle (PUM)-normalized platinum-group element (PGE) and Re patterns of whole rock peridotites from Wudi and Fuxin. (a) Wudi peridotites display variable depletions in Re and the platinum-group PGE (PPGE: Pt and Pd), relative to the iridium-group PGE (IPGE: Os, Ir and Ru), with one sample showing Re enrichment. The patterns of the Fuxin peridotites, along with their Os isotopic compositions, can be divided into four groups: Group 1, Re–PPGE depletion relative to IPGE with low $^{187}Os/^{188}Os$ of 0.1117 to 0.1174 (b); Group 2, Re–PPGE depletion relative to IPGE with high $^{187}Os/^{188}Os$ greater than 0.1214 (b); Group 3, relatively flat PGE patterns also with high $^{187}Os/^{188}Os$ (c); and Group 4, Re–PPGE enrichment relative to IPGE with high $^{187}Os/^{188}Os$ (c). Group 1 peridotites have significant depletions in PPGE relative to IPGE, consistent with high degrees of melt depletion. Groups 2, 3 and 4 peridotites experienced variable degrees of melt–peridotite reaction. See more discussion in text.
PUM values are from Becker et al. (2006).

Formation of dense, lower crustal eclogites and garnet clinopyroxenites, during Mesozoic crustal thickening, gave rise to gravitational instability through which the lower portion of lithosphere may have foundered en masse into the asthenosphere, leading to the production of new lithospheric mantle by passive upwelling and melting of hot asthenospheric material. This sequence of events is recorded in the Late Jurassic Xinglonggou high-Mg andesites, and later in the Early Cretaceous Sihetun high-Mg basalts, which have been interpreted to be derived

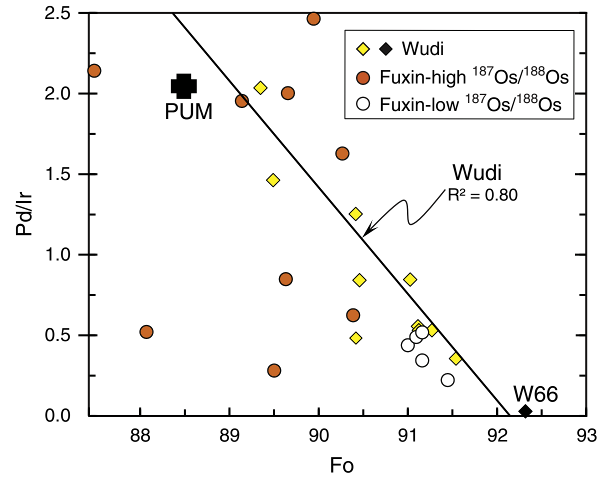

Fig. 4. Whole rock Pd/Ir versus forsterite content (Fo) for peridotitic olivines from Wudi and Fuxin. The Wudi peridotites form a negative correlation consistent with melt depletion. By contrast, the Fuxin peridotites with high $^{187}Os/^{188}Os$ (Groups 2, 3 and 4) show no apparent trend (two samples have highly elevated Pd/Ir ratios (Table 1) and plot off the diagram). Low-$^{187}Os/^{188}Os$ samples (Group 1) have low Pd/Ir and high Fo (>91) and likely experienced high-degrees of melt depletion.
Primitive upper mantle (PUM) values are from Becker et al. (2006) (for Pd/Ir) and McDonough and Sun (1995) (using bulk Mg# for Fo).

from melting of eclogitic lower crust and mantle that was hybridized by eclogitic melts, respectively (Gao et al., 2004, 2008). Moreover, the Fuxin alkali basalts were derived by melting of asthenospheric mantle at a shallow depth (<65 km; Zhang and Zheng, 2003), implying an already thinned lithosphere by the time of eruption (~100 Ma). Given that Fuxin, Xinglonggou and Sihetun are proximal to one another (Fig. 1), these observations suggest that the original Late Archean–Early Paleoproterozoic (≥2.3 Ga) lithospheric mantle was, at least partially removed by density foundering/delamination and replaced by Mesozoic lithospheric mantle. Furthermore, this process had already begun by the Late Jurassic; by ~100 Ma, when the Fuxin basalts erupted, both remnants of the original Precambrian lithospheric mantle and newly-accreted Mesozoic lithospheric mantle coexisted, probably indicating the termination of lithospheric removal/thinning. Moreover, melt–peridotite reaction is widely recorded by Fe-enrichment within the Fuxin peridotites (Zheng et al., 2007; this study).

On the southern margin of the NCC, the Yangtze Craton collided with the southern NCC, leading to the formation of the Triassic Qinling–Dabie Orogenic Belt, as well as the formation of the Tan–Lu fault (Fig. 1; Yin and Nie, 1993). This massive collision also caused lithospheric shortening and thickening in the southern NCC, as evidenced by the presence of Triassic lower crustal eclogite and garnet clinopyroxenite xenoliths (e.g., Xinyang, Zheng et al., 2005; Xu-Huai, Xu et al., 2006). Density foundering/delamination may have occurred more rapidly and extensively in regions close to the collisional boundaries, where a higher degree of lithospheric thickening had occurred. This is consistent with the proposed occurrence of lithospheric thinning in the southeastern NCC prior to the Late Triassic (Yang et al., 2010), while the Late Triassic (~220 Ma) eclogites and garnet clinopyroxenites remained within the interior of the eastern NCC during the Early Cretaceous (Xu et al., 2006). In addition, the numerous Early Cretaceous mantle-derived rocks (e.g., Fangcheng basalts, Zhang et al., 2002; Jiaodong mafic dykes, Yang et al., 2004; Feixian basalts/picrites, Gao et al., 2008; Laiwu-Zibo high Mg diorites, Xu et al., 2008) have crustal-like Sr–Nd isotopic signatures ($^{87}Sr/^{86}Sr(t) = 0.705$ to 0.711, and $\varepsilon Nd(t) = -21$ to -4.0), indicative of incorporation of continental middle-lower crust in their mantle sources, and, thus, marking an ongoing process of lithospheric removal (Huang et al., 2007). By the Late Cretaceous, mantle-derived rocks (e.g., Jiaozhou alkali basalts, Yan et al., 2003; Junan alkali basanites, Ying et al., 2006; Qingdao mafic dykes, Zhang

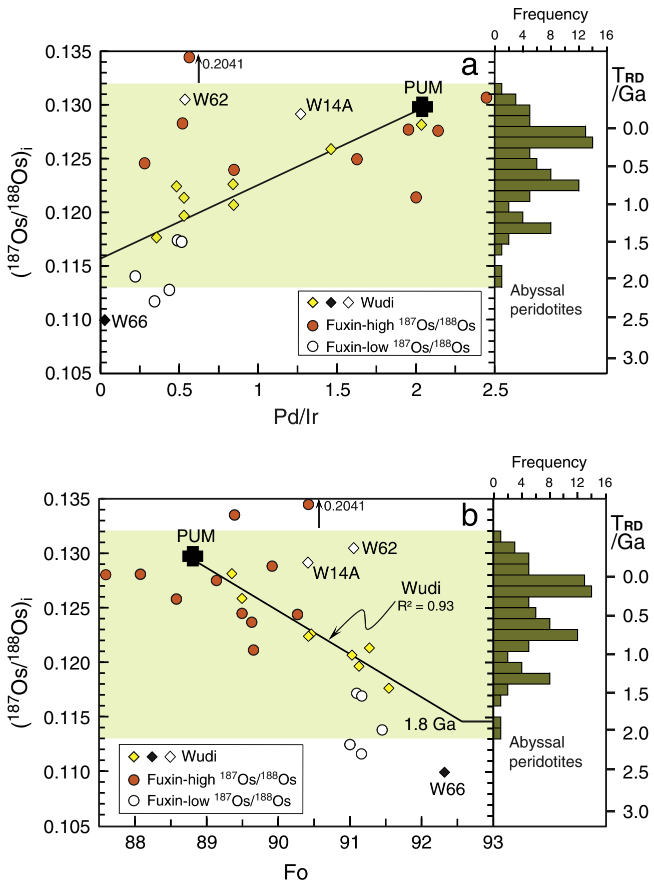

Fig. 5. a–b. Initial $^{187}Os/^{188}Os$ versus (a) Pd/Ir and (b) forsterite content (Fo) for peridotites from Wudi and Fuxin. In panel a, the solid line represents the trend of ancient melt depletion for the Wudi peridotites, excluding the two samples W14A and W62 that may have had overprinting due to low Os concentrations (0.36 and 0.15 ppb, respectively). By contrast, the high-$^{187}Os/^{188}Os$ Fuxin peridotites (Groups 2, 3 and 4) show no apparent trend; two samples have highly elevated Pd/Ir ratios (Table 1) and are not plotted. The low-$^{187}Os/^{188}Os$ Fuxin peridotites (Group 1) have low Pd/Ir, which likely resulted from ancient high-degree melting. In panel b, by excluding the low-Os samples W14A and W62, the Wudi peridotites form a linear correlation yielding an Os model age of 1.8 ± 0.3 Ga, assuming peridotites lose all Re at Fo = 92.5 ± 0.5. The harzburgite W66 having the highest Fo of 92.3 and lowest Pd/Ir of 0.03 yields an older Re-depleted Os model age (T_{RD}) of 2.5 Ga. The low-$^{187}Os/^{188}Os$ Fuxin peridotites yield T_{RD} ages of 1.5 to 2.3 Ga, whereas the high-$^{187}Os/^{188}Os$ samples plot within the range of abyssal peridotites which is illustrated as histograms on the right of each panel and shaded fields on the left of each panel. T_{RD} are calculated using a chondritic mantle with $^{187}Os/^{188}Os$ of 0.1270 and $^{187}Re/^{188}Os$ of 0.402 (Shirey and Walker, 1998). Initial $^{187}Os/^{188}Os$ is calculated at the time of host basalt eruption using the measured $^{187}Re/^{188}Os$ (Table 1).
Primitive upper mantle (PUM): Becker et al. (2006) (for Pd/Ir), Meisel et al. (2001) (for $^{187}Os/^{188}Os$) and McDonough and Sun (1995) (using bulk Mg# for Fo). Abyssal peridotite data are from Parkinson et al. (1998), Brandon et al. (2000), Standish et al. (2002), Harvey et al. (2006), and Liu et al. (2008).

et al., 2008b) were primarily formed via melting of asthenospheric mantle similar to Cenozoic basalts in the eastern NCC (Lee et al., 2006; Peng et al., 1986). This suggests that the major lithospheric thinning had ended by this time. Thus, in the southern portion of the eastern NCC, Phanerozoic lithospheric removal and replacement, via density foundering, initiated at the collisional boundary in the Triassic and then migrated to the interior in the Early Cretaceous.

The discussion above highlights the role of density foundering/delamination in the removal and replacement of deep lithosphere in the eastern NCC, but this process alone cannot account for all of the observations in this study and in the literature. The foundering of eclogitic lower crust and underlying lithospheric mantle implies complete removal of old lithosphere and subsequent replacement by juvenile lithosphere (Kay and Kay, 1993). However, mantle xenoliths entrained in Cretaceous lavas (e.g., Laiwu, Gao et al., 2008; Qingdao, Zhang et al., 2011; Fuxin, this study) and even Cenozoic lavas (Kuandian, Wu et al., 2006; Wudi, this study) that are far removed from the Tan–Lu fault contain remnants of original Precambrian, more refractory lithospheric mantle. By comparison, mantle xenoliths/xenocrysts in Cretaceous lavas erupted close to the fault have changed in composition through time, for example from pyroxenite xenoliths and low-Fo (88–91) olivine xenocrysts beneath Fangcheng (125 Ma; Zhang et al., 2002, 2007) and websterite xenoliths and high-Fo (92–93) olivine xenocrysts beneath Feixian (119 Ma; Pei et al., 2004; Gao et al., 2008; Xu et al., 2013b) in the Early Cretaceous, to lherzolite xenoliths beneath Junan (67 Ma; Ying et al., 2006) in the Late Cretaceous.

In the Early Cretaceous, these mantle rocks/minerals document the transitional modification stage of the original Precambrian lithospheric mantle, thus marking the ongoing destruction of the lithospheric mantle beneath this region, while in the Late Cretaceous, we interpret the predominantly fertile lherzolites to represent the Phanerozoic lithospheric mantle that was newly formed after thinning, as sampled by many mantle xenoliths carried in Cenozoic basalts in the eastern NCC (Fig. 1). This is particularly true of those erupted close to the fault (e.g., Chu et al., 2009; Xiao et al., 2010; Zhang et al., 2007). This suggests that density foundering/delamination did not cause complete removal of old lithosphere beneath the eastern NCC, and it is likely to have occurred locally, where significant shortening and thickening of lithosphere occurred proximal to collisional boundaries. This also suggests that the Triassic-initiated Tan–Lu fault served as a conduit of hot material, and accelerated lithospheric removal and replacement through thermo-mechanical erosion. In addition, intensive magmatism, regional extension and gold mineralization in the Early Cretaceous have been interpreted to have resulted from Paleo-Pacific plate subduction, indicating significant removal of old lithosphere during this period (Zhu et al., 2012a,b). Further, the interaction between peridotite and melt/fluid is observed in fertile mantle peridotites (e.g., Xu et al., 2013b; Zhang et al., 2007; Zheng et al., 2007; this study) and water-enriched, lithospheric mantle-derived basalts (Xia et al., 2013) erupted in the Early Cretaceous in the eastern NCC. This implies that melt/fluid–peridotite interaction processes may have modified the chemical composition of lithospheric mantle by Fe-enrichment and/or hydration, attenuated its physical properties (e.g., by increasing density and/or decreasing viscosity), and ultimately assisted removal of lithospheric mantle.

Collectively, lithospheric mantle removal and replacement during the Phanerozoic in the entire eastern NCC initiated at collisional boundaries and then migrated to the interior via density foundering with the aid of melt–peridotite interaction. Thermo-mechanical erosion associated with the Tan–Lu fault may have further contributed to lithospheric thinning.

Overall, the NCC experienced lithospheric removal in both the Paleoproterozoic (~1.8 Ga) and Phanerozoic. These removal events were primarily associated with the collisional orogens. The Paleoproterozoic removal presumably resulted from the western–eastern collisions that amalgamated the NCC in the Paleoproterozoic (Liu et al., 2010, 2011, 2012; this study). The Phanerozoic removal may have been spatially associated with the collisional orogens on the northern and southern margins and the Tan–Lu fault, as well as the Paleo-Pacific plate subduction. In this context, it is noteworthy that peridotites carried in Cenozoic alkali basalts from the southeastern margin of the Siberia Craton at Tok (located to the north of the NCC along the Xing-Meng Orogenic Belt; Fig. 1; see Fig. 1 of Ionov et al. (2005) for the locality of Tok) exhibit remarkable similarities in chemical compositions (including a large range of Fo values and PGE patterns; Ionov et al., 2005, 2006a) and Os isotope compositions (Ionov et al., 2006a) to the Fuxin peridotites. Given their similar tectonic settings (both close to the Xing-Meng collisional orogen and Paleo-Pacific plate subduction), it is envisioned that similar lithospheric

Table 2
Summary of the main tectonic events within the North China Craton (NCC).

Time before present	Events
ca. 3.8 to 2.5 Ga	Formation of micro-continents that later assembled to form the NCC; the Archean crust was coupled with the underlying Archean lithospheric mantle sampled by peridotites in Ordovician kimberlites
ca. 2.1 to 1.9 Ga	Formation of the Jiao-Liao-Ji Belt via the collision of the northern Longgang and southern Rangrim blocks to form the eastern NCC
ca. 1.95 Ga	Formation of the Khondalite Belt via the collision of the Yinshan and Ordos blocks to form the western NCC
ca. 1.85 Ga	Amalgamation of the NCC along the Trans-North China Orogen (TNCO) via continent–continent collision between the Eastern and Western blocks; lithospheric mantle replacement occurred in the northern TNCO
ca. 450 to 360 Ma	Formation of the Qilian Orogen to the west of the NCC
ca. 300 to 240 Ma	Formation of the Xing-Meng Orogenic Belt (the eastern extension of the Central Asian Orogenic Belt) via the collision of the NCC and Siberian Craton, causing crustal shortening and thickening on the margins of both cratons
260 to 225 Ma	Formation of the Qinling–Dabie–Sulu Orogenic Belt via the collision of the NCC and Yangtze Craton, initiating the Tan–Lu fault and causing crustal shortening and thickening on the south-eastern margin of the NCC
220 Ma	Lithospheric thinning and replacement in the south-eastern NCC
ca. 190 Ma	Onset of Paleo-Pacific plate subduction beneath eastern China
160–120 Ma	Density foundering of eclogitic lower crust on the northern margin of the eastern NCC
130–110 Ma	Transitional modification of the Precambrian lithospheric mantle in the southern portion of the eastern NCC
100 Ma	Evidence for thinned lithosphere (<65 km) on the northern margin of the eastern NCC (from Fuxin)
80–0 Ma	Evidence for widespread thin, fertile, Phanerozoic lithospheric mantle beneath eastern NCC with some remnants of original Precambrian lithospheric mantle distant from the Tan–Lu fault; observation of similar lithospheric mantle structure on the south-eastern margin of the Siberian Craton

Note: See text for references.

thinning and replacement occurred on the southeastern margin of the Siberia Craton during the Mesozoic–Cenozoic era, as suggested by Ionov et al. (2006b).

6. Conclusions

Our data show that the Wudi peridotites, carried in Pleistocene (<1 Ma) alkali nephelinites, experienced melt depletion primarily during the Paleoproterozoic (~1.8 Ga), while an Archean Os model age (T_{RD} = 2.5 Ga) for one xenolith indicates incorporation of a minor component of Archean lithospheric mantle. This observation suggests that a previously unrecognized Paleoproterozoic orogenic event led to the removal and replacement of most of the original Archean lithospheric mantle in the vicinity of the Bohai Sea. By contrast, the Fuxin peridotites, carried in ~100 Ma old basalts and located on the northern edge of the eastern NCC, record coexistence of both ancient (≥2.3 Ga) and modern lithospheric mantle components, suggesting that the original Late Archean–Early Paleoproterozoic lithospheric mantle was, at least partially, removed and replaced prior to 100 Ma beneath this area. Combined with literature data, our new results show that removal of the original Archean lithosphere occurred within Proterozoic collisional orogens, and that replacement of Precambrian lithosphere during the Mesozoic may have been spatially associated with the collisional boundaries and the Tan–Lu fault, as well as the onset of Paleo-Pacific plate subduction.

Acknowledgments

We thank Will Junkin and Tess van Orden for making olivine mounts, and Phil Piccoli for help with obtaining the electron microprobe data. We also thank Costanza Bonadiman for inviting us to submit this manuscript to the Tectonophysics Special Issue, and Editor Laurent Jolivet, Guest Editor Gianluca Bianchini, Judith Coggon, and Dmitri Ionov for their editing, constructive comments and/or suggestions that further improved this manuscript. This work was supported by the U.S. NSF (Grants EAR 0635671 and 0911096 to R.L.R. and R.J.W.), and the China NSF (Grants 41330206 and 41272077 to W.L.X.).

Appendix A. Supplementary data

Supplementary data to this article can be found online at http://dx.doi.org/10.1016/j.tecto.2014.05.009.

References

Becker, H., Horan, M.F., Walker, R.J., Gao, S., Lorand, J.P., Rudnick, R.L., 2006. Highly siderophile element composition of the Earth's primitive upper mantle: constraints from new data on peridotite massifs and xenoliths. Geochim. Cosmochim. Acta 70, 4528–4550.
Bernstein, S., Kelemen, P.B., Hanghøj, K., 2007. Consistent olivine Mg# in cratonic mantle reflects Archean mantle melting to the exhaustion of orthopyroxene. Geology 35, 459–462.
Birck, J.L., RoyBarman, M., Capmas, F., 1997. Re–Os isotopic measurements at the femtomole level in natural samples. Geostand. Newslett. J. Geostand. Geoanal. 21, 19–27.
Brandon, A.D., Snow, J.E., Walker, R.J., Morgan, J.W., Mock, T.D., 2000. ^{190}Pt–^{186}Os and ^{187}Re–^{187}Os systematics of abyssal peridotites. Earth Planet. Sci. Lett. 177, 319–335.
Chen, L., 2010. Concordant structural variations from the surface to the base of the upper mantle in the North China Craton and its tectonic implications. Lithos 120, 96–115.
Chen, D., Peng, Z., 1985. K–Ar ages and Pb, Sr isotopic characteristics of Cenozoic volcanic rocks in Shandong, China (in Chinese). Geochimica 4, 293–303.
Chu, Z.Y., Wu, F.Y., Walker, R.J., Rudnick, R.L., Pitcher, L., Puchtel, I.S., Yang, Y.H., Wilde, S.A., 2009. Temporal evolution of the lithospheric mantle beneath the eastern North China Craton. J. Petrol. 50, 1857–1898.
Cohen, A.S., Waters, F.G., 1996. Separation of osmium from geological materials by solvent extraction for analysis by thermal ionisation mass spectrometry. Anal. Chim. Acta. 332, 269–275.
Gao, S., Rudnick, R.L., Carlson, R.W., McDonough, W.F., Liu, Y.S., 2002. Re–Os evidence for replacement of ancient mantle lithosphere beneath the North China Craton. Earth Planet. Sci. Lett. 198, 307–322.
Gao, S., Rudnick, R.L., Yuan, H.L., Liu, X.M., Liu, Y.S., Xu, W.L., Ling, W.L., Ayers, J., Wang, X.C., Wang, Q.H., 2004. Recycling lower continental crust in the North China Craton. Nature 432, 892–897.
Gao, S., Rudnick, R.L., Xu, W.L., Yuan, H.L., Liu, Y.S., Walker, R.J., Puchtel, I.S., Liu, X.M., Huang, H., Wang, X.R., Yang, J., 2008. Recycling deep cratonic lithosphere and generation of intraplate magmatism in the North China Craton. Earth Planet. Sci. Lett. 270, 41–53.
Griffin, W.L., Zhang, A.D., O'Reilly, S.Y., Ryan, C.G., 1998. Phanerozoic evolution of the lithosphere beneath the Sino–Korean Craton. In: Flower, M., Chung, S.-L., Lo, C.-H., Lee, T.-Y. (Eds.), Mantle Dynamics and Plate Interactions in East Asia. Geodynamics Series, 27. American Geophysical Union, Washington, D.C., pp. 107–126.
Handler, M.R., Bennett, V.C., Esat, T.M., 1997. The persistence of off-cratonic lithospheric mantle: Os isotopic systematics of variably metasomatised southeast Australian xenoliths. Earth and Planetary Science Letters 151, 61–75.
Harvey, J., Gannoun, A., Burton, K.W., Rogers, N.W., Alard, O., Parkinson, I.J., 2006. Ancient melt extraction from the oceanic upper mantle revealed by Re–Os isotopes in abyssal peridotites from the Mid-Atlantic ridge. Earth Planet. Sci. Lett. 244, 606–621.
Huang, F., Li, S.-G., Yang, W., 2007. Contributions of the lower crust to Mesozoic mantle-derived mafic rocks from the North China Craton: implications for lithospheric thinning. Geol. Soc. Lond. Spec. Publ. 280, 55–75.
Ionov, D.A., Chanefo, I., Bodinier, J.L., 2005. Origin of Fe-rich lherzolites and wehrlites from Tok, SE Siberia by reactive melt percolation in refractory mantle peridotites. Contrib. Mineral. Petrol. 150, 335–353.
Ionov, D.A., Shirey, S.B., Weis, D., Brugmann, G., 2006a. Os–Hf–Sr–Nd isotope and PGE systematics of spinel peridotite xenoliths from Tok, SE Siberian Craton: effects of pervasive metasomatism in shallow refractory mantle. Earth Planet. Sci. Lett. 241, 47–64.
Ionov, D.A., Chazot, G., Chauvel, C., Merlet, C., Bodinier, J.L., 2006b. Trace element distribution in peridotite xenoliths from Tok, SE Siberian Craton: a record of pervasive, multi-stage metasomatism in shallow refractory mantle. Geochim. Cosmochim. Acta 70, 1231–1260.

Jordan, T.H., 1988. Structure and formation of the continental lithosphere. In: Menzies, M.A., Cox, K. (Eds.), Oceanic and continental lithosphere; similarities and differences. Journal of Petrology, pp. 11–37 (Special Lithosphere Issue).
Kay, R.W., Kay, S.M., 1993. Delamination and delamination magmatism. Tectonophysics 219, 177–189.
Lee, Y.-T., Chen, J.-C., Shih, J.-Y., Juang, W.-S., Yang, H.-J., Huang, S.-W., Lin, M.-L., 2006. Geochemistry of Cenozoic basaltic rocks from Shandong Province and its implication for mantle process in North China. Geochem. J. 40, 579–596.
Li, S.Z., Zhao, G.C., Santosh, M., Liu, X., Dai, L.M., 2011. Palaeoproterozoic tectonothermal evolution and deep crustal processes in the Jiao-Liao-Ji Belt, North China Craton: a review. Geol. J. 46, 525–543.
Liu, C.Z., Snow, J.E., Hellebrand, E., Brugmann, G., von der Handt, A., Buchl, A., Hofmann, A.W., 2008. Ancient, highly heterogeneous mantle beneath Gakkel ridge, Arctic Ocean. Nature 452, 311–316.
Liu, J., Rudnick, R.L., Walker, R.J., Gao, S., Wu, F.Y., Piccoli, P.M., 2010. Processes controlling highly siderophile element fractionations in xenolithic peridotites and their influence on Os isotopes. Earth Planet. Sci. Lett. 297, 287–297.
Liu, J., Rudnick, R.L., Walker, R.J., Gao, S., Wu, F.-Y., Piccoli, P.M., Yuan, H., Xu, W.-L., Xu, Y.-G., 2011. Mapping lithospheric boundaries using Os isotopes of mantle xenoliths: an example from the North China Craton. Geochimica et Cosmochimica Acta 75, 3881–3902.
Liu, J., Carlson, R.W., Rudnick, R.L., Walker, R.J., Gao, S., Wu, F.-Y., 2012. Comparative Sr–Nd–Hf–Os–Pb isotope systematics of xenolithic peridotites from Yangyuan, North China Craton: additional evidence for a Paleoproterozoic age. Chem. Geol. 332–333, 1–14.
Luo, D., Chen, L.H., Zeng, G., 2009. Genesis of intra-continental strongly alkaline volcanic rocks: a case study of Dashan nephelinites in Wudi, Shandong Province, North China. Acta Petrol. Sin. 25 (2), 311–319.
McDonough, W.F., Sun, S.S., 1995. The composition of the earth. Chem. Geol. 120, 223–253.
Meisel, T., Walker, R.J., Irving, A.J., Lorand, J.P., 2001. Osmium isotopic compositions of mantle xenoliths: a global perspective. Geochim. Cosmochim. Acta 65, 1311–1323.
Menzies, M.A., Fan, W.-M., Zhang, M., 1993. Paleozoic and Cenozoic lithoprobes and the loss of >120 km of Archean lithosphere, Sino–Korean Craton, China. In: Prichard, H.M., Alabaster, H.M., Harris, T., Neary, C.R. (Eds.), Magmatic Processes and Plate Tectonics. Geological Soc., London, pp. 71–81.
Nier, A.O., 1950. A redetermination of the relative abundances of the isotopes of carbon, nitrogen, oxygen, argon, and potassium. Phys. Rev. 77, 789–793.
Parkinson, I.J., Hawkesworth, C.J., Cohen, A.S., 1998. Ancient mantle in a modern arc: osmium isotopes in Izu–Bonin–Mariana forearc peridotites. Science 281, 2011–2013.
Pearson, D.G., Canil, D., Shirey, S.B., 2014. 3.5 — mantle samples included in volcanic rocks: xenoliths and diamonds. In: Holland, H.D., Turekian, K.K. (Eds.), Treatise on Geochemistry (2nd Edition). Elsevier, Oxford, pp. 169–253.
Pei, F.P., Xu, W.L., Wang, Q.H., Wang, D.Y., 2004. Mesozoic basalt and mineral chemistry of the mantle-derived xenocrysts in Feixian, Western Shandong, China: Constraints on nature of Mesozoic lithospheric mantle. Geological Journal of China Universities 10, 88–97.
Peng, Z.C., Zartman, R.E., Futa, K., Chen, D.G., 1986. Pb-, Sr- and Nd-isotopic systematics and chemical characteristics of Cenozoic basalts, eastern China. Chem. Geol. 59, 3–33.
Rehkämper, M., Halliday, A.N., 1997. Development and application of new ion-exchange techniques for the separation of the platinum group and other siderophile elements from geological samples. Talanta 44, 663–672.
Shirey, S.B., Walker, R.J., 1998. The Re–Os isotope system in cosmochemistry and high-temperature geochemistry. Annu. Rev. Earth Planet. Sci. 26, 423–500.
Standish, J.J., Hart, S.R., Blusztajn, J., Dick, H.J.B., Lee, K.L., 2002. Abyssal peridotite osmium isotopic compositions from Cr-spinel. Geochem. Geophys. Geosyst. 3.
Tian, Y., Zhao, D.P., Sun, R.M., Teng, J.W., 2009. Seismic imaging of the crust and upper mantle beneath the North China Craton. Phys. Earth Planet. Inter. 172, 169–182.
Walker, R.J., Brandon, A.D., Bird, J.M., Piccoli, P.M., McDonough, W.F., Ash, R.D., 2005. ^{187}Os–^{186}Os systematics of Os–Ir–Ru alloy grains from southwestern Oregon. Earth Planet. Sci. Lett. 230, 211–226.
Wu, F.Y., Walker, R.J., Ren, X.W., Sun, D.Y., Zhou, X.H., 2003. Osmium isotopic constraints on the age of lithospheric mantle beneath northeastern China. Chem. Geol. 196, 107–129.
Wu, F.Y., Lin, J.Q., Wilde, S.A., Zhang, X.O., Yang, J.H., 2005. Nature and significance of the Early Cretaceous giant igneous event in eastern China. Earth Planet. Sci. Lett. 233, 103–119.
Wu, F.Y., Walker, R.J., Yang, Y.H., Yuan, H.L., Yang, J.H., 2006. The chemical–temporal evolution of lithospheric mantle underlying the North China Craton. Geochim. Cosmochim. Acta 70, 5013–5034.
Xia, Q.-K., Liu, J., Liu, S.-C., Kovacs, I., Feng, M., Dang, L., 2013. High water content in Mesozoic primitive basalts of the North China Craton and implications on the destruction of cratonic mantle lithosphere. Earth Planet. Sci. Lett. 361, 85–97.
Xiao, Y., Zhang, H.F., Fan, W.M., Ying, J.F., Zhang, J., Zhao, X.M., Su, B.X., 2010. Evolution of lithospheric mantle beneath the Tan–Lu fault zone, eastern North China Craton: evidence from petrology and geochemistry of peridotite xenoliths. Lithos 117, 229–246.
Xu, W.L., Gao, S., Wang, Q.H., Wang, D.Y., Liu, Y.S., 2006. Mesozoic crustal thickening of the eastern North China Craton: evidence from eclogite xenoliths and petrologic implications. Geology 34, 721–724.
Xu, W.L., Hergt, J.A., Gao, S., Pei, F.P., Wang, W., Yang, D.B., 2008. Interaction of adakitic melt–peridotite: implications for the high-Mg# signature of Mesozoic adakitic rocks in the eastern North China Craton. Earth Planet. Sci. Lett. 265, 123–137.
Xu, W.L., Pei, F.P., Wang, F., Meng, E., Ji, W.Q., Yang, D.B., Wang, W., 2013a. Spatial–temporal relationships of Mesozoic volcanic rocks in NE China: constraints on tectonic overprinting and transformations between multiple tectonic systems. J. Asian Earth Sci. 74, 167–193.
Xu, W.L., Zhou, Q.-J., Pei, F.-P., Yang, D.-B., Gao, S., Li, Q.-L., Yang, Y.-H., 2013b. Destruction of the North China Craton: delamination or thermal/chemical erosion? Mineral chemistry and oxygen isotope insights from websterite xenoliths. Gondwana Res. 23, 119–129.
Yan, J., Chen, J., Xie, Z., Zhou, T., 2003. Mantle xenoliths from Late Cretaceous basalt in eastern Shandong Province: new constraint on the timing of lithospheric thinning in eastern China. Chin. Sci. Bull. 48, 2139–2144.
Yang, J.H., Chung, S.L., Zhai, M.G., Zhou, X.H., 2004. Geochemical and Sr–Nd–Pb isotopic compositions of mafic dikes from the Jiaodong Peninsula, China: evidence for vein-plus-peridotite melting in the lithospheric mantle. Lithos 73, 145–160.
Yang, J.H., Wu, F.Y., Chung, S.-L., Lo, C.H., Wilde, S.A., Davis, G.A., 2007. Rapid exhumation and cooling of the Liaonan metamorphic core complex: inferences from ^{40}Ar/^{39}Ar thermochronology and implications for Late Mesozoic extension in eastern North China Craton. Geol. Soc. Am. Bull. 119, 1405–1414.
Yang, J.H., O'Reilly, S., Walker, R.J., Griffin, W., Wu, F.Y., Zhang, M., Pearson, N., 2010. Diachronous decratonization of the Sino–Korean Craton: geochemistry of mantle xenoliths from North Korea. Geology 38, 799–802.
Yin, A., Nie, S., 1993. An indentation model for the North and South China collision and the development of the Tan–Lu and Honam fault systems, eastern Asia. Tectonics 12, 801–813.
Ying, J.F., Zhang, H.F., Kita, N., Morishita, Y., Shimoda, G., 2006. Nature and evolution of late cretaceous lithospheric mantle beneath the eastern North China Craton: constraints from petrology and geochemistry of peridotitic xenoliths from Junan, Shandong Province, China. Earth Planet. Sci. Lett. 244, 622–638.
Zhang, H.F., Zheng, J.P., 2003. Geochemical characteristics and petrogenesis of Mesozoic basalts from the North China Craton: a case study in Fuxin, Liaoning Province. Chin. Sci. Bull. 48, 924–930.
Zhang, H.F., Sun, M., Zhou, X.H., Fan, W.M., Zhai, M.G., Yin, J.F., 2002. Mesozoic lithosphere destruction beneath the North China Craton: evidence from major-, trace-element and Sr–Nd–Pb isotope studies of Fangcheng basalts. Contrib. Mineral. Petrol. 144, 241–253.
Zhang, H.F., Nakamura, E., Sun, M., Kobayashi, K., Zhang, J., Ying, J.F., Tang, Y.J., Niu, L.F., 2007. Transformation of subcontinental lithospheric mantle through peridotite–melt reaction: evidence from a highly fertile mantle xenolith from the North China Craton. Int. Geol. Rev. 49, 658–679.
Zhang, H.F., Goldstein, S.L., Zhou, X.H., Sun, M., Zheng, J.P., Cai, Y., 2008a. Evolution of subcontinental lithospheric mantle beneath eastern China: Re–Os isotopic evidence from mantle xenoliths in Paleozoic kimberlites and Mesozoic basalts. Contrib. Mineral. Petrol. 155, 271–293.
Zhang, J., Zhang, H.-F., Ying, J.-F., Tang, Y.-J., Niu, L.-F., 2008b. Contribution of subducted Pacific slab to Late Cretaceous mafic magmatism in Qingdao region, China: a petrological record. Island Arc 17, 231–241.
Zhang, J., Zhang, H., Kita, N., Shimoda, G., Morishita, Y., Ying, J., Tang, Y., 2011. Secular evolution of the lithospheric mantle beneath the eastern North China Craton: evidence from peridotitic xenoliths from Late Cretaceous mafic rocks in the Jiaodong region, east-central China. Int. Geol. Rev. 53, 182–211.
Zhao, G.C., Sun, M., Wilde, S.A., Li, S.Z., 2005. Late Archean to Paleoproterozoic evolution of the North China Craton: key issues revisited. Precambrian Res. 136, 177–202.
Zheng, J.P., 1999. Mesozoic and Cenozoic Lithospheric Mantle Replacement and Thinning in Eastern China. Press of China University of Geosciences, p. 126.
Zheng, C.Q., Xu, W.L., Wang, D.Y., 1999. The petrology and mineral chemistry of the deep-seated xenoliths in Mesozoic basalt in Fuxin district from western Liaoning. Acta Petrol. Sin. 15 (4), 616–622.
Zheng, J.P., Sun, M., Lu, F.X., Yu, C.M., Wang, F.Z., 2005. Xinyang mafic granulitic xenoliths and its significance for the early Mesozoic lower crustal nature on the south margin of the North China Craton. Acta Petrol. Sin. 21, 91–98.
Zheng, J.P., Griffin, W.L., O'Reilly, S.Y., Yu, C.M., Zhang, H.F., Pearson, N., Zhang, M., 2007. Mechanism and timing of lithospheric modification and replacement beneath the eastern North China Craton: peridotitic xenoliths from the 100 Ma Fuxin basalts and a regional synthesis. Geochim. Cosmochim. Acta 71, 5203–5225.
Zhu, R.-X., Xu, Y.G., Zhu, G., Zhang, H.F., Xia, Q.-K., Zheng, T.Y., 2012a. Destruction of the North China Craton. Sci. China Earth Sci. 55, 1565–1587.
Zhu, R.-X., Yang, J.H., Wu, F.-Y., 2012b. Timing of destruction of the North China Craton. Lithos 149, 51–60.